

# Design to reduce electromagnetic vibration in integral-slot SPM machine considering force modulation effect

ZHU ShengDao<sup>1</sup>, ZHAO WenXiang<sup>1\*</sup>, JI JingHua<sup>1</sup>, LIU GuoHai<sup>1</sup> & LEE Christopher H. T.<sup>2</sup>

<sup>1</sup> School of Electrical and Information Engineering, Jiangsu University, Zhenjiang 212013, China;

<sup>2</sup> School of Electrical and Electronic Engineering, Nanyang Technological University, Singapore 639798, Singapore

Received March 29, 2022; accepted May 20, 2022; published online June 21, 2022

In this paper, two different designs, with dummy slots and bread-loaf magnets techniques, are presented to reduce the electromagnetic vibration in integral-slot surface-mounted permanent-magnet (SPM) machines. Firstly, the stator slotting effect on the magnetic field modulation and radial force modulation is investigated. It reveals the amplitude of the modulated magnetic field and modulated radial force is greatly affected by the slot opening effect, while the spatial order is closely associated with the slot numbers. Subsequently, the dummy slots and bread-loaf magnets design are developed for a 36-slot/12-pole integral-slot SPM machine to reduce the electromagnetic vibration. Finally, two SPM machines, with conventional and bread-loaf magnets, are manufactured. Experimental tests are carried out to validate the theoretical analyses.

**surface-mounted permanent-magnet machine, slot opening width, dummy slots, bread-loaf magnets, vibration reduction.**

**Citation:** Zhu S D, Zhao W X, Ji J H, et al. Design to reduce electromagnetic vibration in integral-slot SPM machine considering force modulation effect. *Sci China Tech Sci*, 2022, 65: 1867–1877, <https://doi.org/10.1007/s11431-022-2089-y>

## 1 Introduction

Surface-mounted permanent-magnet (SPM) machines have received extensive attention in the field of servo systems due to their advantages of high-power density, high efficiency, simple structure, small size, and high-power factor [1–3]. Due to the increasing demand for better electric machines, much attention has been paid to the electromagnetic vibration analysis [4–6].

The vibration of SPM machines is mainly caused by electromagnetic radial forces [7,8]. According to the vibration model proposed by H. Jordan in the 1950s, the vibration displacement of the SPM machine is inversely proportional to the fourth power of the radial force spatial order [9,10]. It can be inferred that low-order radial forces play a critical role in vibration generation. In addition, the lowest order of radial force in the SPM machine is equal to the greatest common

divisor (GCD) of the pole and slot numbers [11]. The lowest order of radial force in integral-slot SPM machines is relatively higher than that in fractional-slot machines. Consequently, the vibration performances of integral-slot SPM machines are better than that of fractional-slot counterparts. As compared with the fractional-slot SPM machines, the integral-slot SPM machines have a lower magnetic field and radial force harmonic content [12]. Therefore, the integral-slot SPM machine has the potential to be applied on occasions with strict requirements for vibration and noise.

Although the amplitude of the lowest non-zeroth-order radial force in integral-slot SPM machines is relatively large, the non-zeroth-order radial force has an insignificant effect on the vibration due to its high spatial order. It is found the critical vibration mode of integral-slot SPM machines presents the breathing mode, and the zeroth-order radial force is the dominant factor in the breathing vibration generation [13–15]. However, the frequency of the zeroth-order radial force is zero, which can only produce static displacement but

\*Corresponding author (email: [zwx@ujs.edu.cn](mailto:zwx@ujs.edu.cn))

not dynamic vibration. Subsequently, the force modulation effect was studied in refs. [16–18], which disclosed the high-order radial forces could be modulated to low-order ones by stator teeth. The breathing mode vibration is produced by the slot number order (i.e.,  $Q$ th-order) radial force, which can be modulated to zeroth-order radial force by stator teeth [18]. According to the force modulation effect, high-order radial forces can produce low-order vibrations. In addition, the  $Q$ th-order radial force has a larger contribution to the vibrations than the primitive zeroth-order. The effect of slot opening width on the ratio of two different radial forces to vibration was studied in refs. [14,18]. However, the influence of slot opening width of SPM machines on the amplitude of the modulated radial force has not been carried out yet.

The most effective method to suppress the vibrations of integral-slot SPM machines is to reduce the  $Q$ th-order radial force rather than the lowest order radial force, which is different from the vibration reduction measures for fractional-slot SPM machines [19,20]. Although many reduction measures of radial force and vibration in SPM machines have been reported in refs. [21–24], the method and principle of vibration reduction from the perspective of the radial force modulation effect have not been thoroughly studied. Hence, the main contribution of this paper is to propose two different vibration reduction designs, where the radial force modulation effect will be considered. The stator teeth play the role of a modulator in the process of radial force modulation. The first one is to restrict the modulation from the  $Q$ th-order radial force to the zeroth-order radial force by modifying the stator modulator structure. The second one is to suppress the magnetic field source of the  $Q$ th-order radial force. Moreover, their vibration reduction effect will also be compared and analyzed.

In this paper, two different designs are presented to reduce vibrations for integral-slot SPM machines, where the radial force modulation effect is considered. This paper is structured as follows. In Sect. 2, the stator slotting effect on the magnetic field modulation and radial force modulation will be investigated. In Sects. 3 and 4, the dummy slots and bread-loaf magnets designs will be proposed, and their vibration reduction principles will be elaborated. Next, the prototypes of the 36-slot/12-pole integral-slot SPM machine will be fabricated, and the experimental verifications will be given in Sect. 5. Finally, conclusions will be drawn in Sect. 6.

## 2 Modulation effect on radial force

The modulation effect in SPM machines attributes to the stator slotting effect. The influence of the modulation effect on radial force can be studied from two aspects, i.e., the magnetic field modulation and the radial force modulation.

### 2.1 Magnetic field modulation

The PM magnetomotive force (MMF) of the SPM machine is a function of time and angular position, and its Fourier series expansion can be expressed as

$$F_{\text{pm}} = \sum_{v_p} F_p \cos(v_p p \theta - 2\pi v_p f_e t), \quad (1)$$

where  $F_{\text{pm}}$  is the PM MMF,  $F_p$  and  $v_p$  are the amplitude and spatial order of PM MMF,  $p$  is the pole-pair number,  $f_e$  is the electrical frequency,  $\theta$  and  $t$  are the angular position and time. Due to the stator slotting effect of the SPM machine, the air-gap permeance is no longer a constant, and its Fourier series can be expressed as

$$\lambda_{\text{gap}} = \lambda_0 + \sum_k \lambda_k \cos(kQ\theta), \quad (2)$$

where  $\lambda_{\text{gap}}$  is the air-gap permeance,  $\lambda_0$  is the DC component of the air-gap permeance,  $\lambda_k$  is the amplitude of the  $k$ -order permeance,  $k$  is a positive integer, and  $Q$  is the stator slot number. The radial PM flux density can be expressed as

$$\begin{aligned} B_{\text{pm}} &= F_{\text{pm}} \cdot \lambda_{\text{gap}} \\ &= \sum_{v_p} F_p \cos(v_p p \theta - 2\pi v_p f_e t) \cdot \left[ \lambda_0 + \sum_k \lambda_k \cos(kQ\theta) \right] \\ &= \underbrace{\sum_{v_p} B_p \cos(v_p p \theta - 2\pi v_p f_e t)}_{\text{Primitive harmonics}} \\ &\quad + \underbrace{\sum_{k=1}^{\infty} \sum_{v_p} B_{\text{pk}} \cos(|v_p p \pm kQ| \theta - 2\pi v_p f_e t)}_{\text{Modulated harmonics}}, \end{aligned} \quad (3)$$

where  $B_{\text{pm}}$  is the radial PM flux density,  $B_p$  and  $B_{\text{pk}}$  are amplitudes of primitive and modulated PM flux density harmonics. After the magnetic field modulation by stator teeth, apart from the primitive harmonics with spatial order  $v_p p$ , modulated harmonics emerge with the spatial order of  $|v_p p \pm kQ|$ . The armature reaction flux density can be expressed as

$$\begin{aligned} B_{\text{arm}} &= F_{\text{arm}} \cdot \lambda_{\text{gap}} \\ &= \sum_{v_s} F_s \cos(v_s u_t \theta - 2\pi \mu f_e t) \cdot \left[ \lambda_0 + \sum_k \lambda_k \cos(kQ\theta) \right] \\ &= \underbrace{\sum_{v_s} B_s \cos(v_s u_t \theta - 2\pi \mu f_e t)}_{\text{Primitive harmonics}} \\ &\quad + \underbrace{\sum_{k=1}^{\infty} \sum_{v_s} B_{\text{sk}} \cos[(v_s u_t \pm kQ)\theta - \mu 2\pi f_e t]}_{\text{Modulated harmonics}}, \end{aligned} \quad (4)$$

where  $B_{\text{arm}}$  is the armature reaction flux density,  $F_{\text{arm}}$  is the armature reaction MMF,  $F_s$  and  $v_s$  are the amplitude and spatial order of armature reaction MMF harmonics,  $u_t$  is the number of unit machines,  $\mu$  is  $\pm 1$ , and it represents the rotation direction of the armature reaction MMF harmonics. In addition to the primitive harmonics with spatial order  $v_s u_t$ , modulated harmonics with spatial order  $|v_s u_t \pm kQ|$  appear. These emerging modulated harmonics will inevitably affect the radial force harmonics of SPM machines.

The radial force density can be calculated by the Maxwell stress tensor method as

$$p_r(\theta, t) = \frac{B_r^2(\theta, t) - B_t^2(\theta, t)}{2\mu_0} \approx \frac{B_r^2(\theta, t)}{2\mu_0}, \quad (5)$$

where  $p_r$  is the radial force density,  $B_r$  and  $B_t$  are the radial and tangential air-gap flux density, and  $\mu_0$  is the vacuum permeability. The effect of tangential flux density harmonics on radial forces is generally ignored due to their insignificant amplitude [24,25]. The radial force density can be regarded as the result of the interaction between two radial flux density harmonics. The radial flux density consists of PM flux density and armature reaction flux density, and it can be written as

$$B_r(\theta, t) = B_{pm}(\theta, t) + B_{arm}(\theta, t). \quad (6)$$

Substituting eqs. (3), (4), and (6) into eq. (5), the radial force density can be obtained as

$$P_r(\theta, t) = \frac{1}{2\mu_0}(B_{pm}^2 + B_{arm}^2 + 2B_{pm}B_{arm})$$

$$= \frac{1}{2\mu_0} \left\{ \sum_{v_p} B_{p_p} \cos(v_p p \theta - 2\pi v_p f_e t) + \sum_{k=1}^{\infty} \sum_{v_p} B_{p_{pk}} \cos[(v_p p \pm kQ)\theta - 2\pi v_p f_e t] \right\}^2$$

$$+ \frac{1}{2\mu_0} \left\{ \sum_{v_s} B_{s_s} \cos(v_s u_t \theta - 2\pi \mu f_e t + \varphi_{v_s}) + \sum_{k=1}^{\infty} \sum_{v_s} B_{s_{sk}} \cos[(v_s u_t \pm kQ)\theta - \mu 2\pi f_e t] \right\}^2$$

$$+ \frac{1}{\mu_0} \left\{ \sum_{v_p} B_{p_p} \cos(v_p p \theta - 2\pi v_p f_e t) + \sum_{k=1}^{\infty} \sum_{v_p} B_{p_{pk}} \cos[(v_p p \pm kQ)\theta - v_p 2\pi f_e t] \right\}$$

$$\times \left\{ \sum_{v_s} B_{s_s} \cos(v_s u_t \theta - \mu 2\pi f_e t + \varphi_{v_s}) + \sum_{k=1}^{\infty} \sum_{v_s} B_{s_{sk}} \cos[(v_s u_t \pm kQ)\theta - 2\pi \mu f_e t] \right\}. \quad (7)$$

The slot number of the integral-slot SPM machine is a multiple of the pole-pair number, namely  $Q=kp$ . Therefore, the magnetic field modulation effect will not change the spatial order distribution of the flux density harmonics, but it will change the amplitude of each flux density harmonic. Consequently, the radial force will not add new harmonics, but it will change the amplitude of the radial force harmonics. It should be noted that this phenomenon is only applicable to integral-slot SPM machines. If it is a fractional-slot SPM machine, the consequence will be different [20].

### 2.2 Radial force modulation

In the traditional vibration model of SPM machines, the stator is usually equivalent to a cylindrical structure. The

static and dynamic vibration displacements of the equivalent cylinder can be expressed by Jordan’s formula as

$$\begin{cases} Y_v^s(v=0) = -\frac{R_i R_y}{E h_y} \sigma_v, \\ Y_v^s(v \geq 2) = \frac{12 R_i R_y^3}{E h_y^3 (v^2 - 1)^2} \sigma_v, \\ Y_v^d = Y_v^s \left[ (1 - f_v^2 / f_m^2)^2 + 4 \zeta_m^2 f_v^2 / f_m^2 \right]^{-1/2}, \end{cases} \quad (8)$$

where  $Y_v^s$  and  $Y_v^d$  are the static vibration displacements and dynamic vibration displacements,  $R_i$  is the inner radius of the stator,  $R_y$  is the radius of the stator yoke,  $h_y$  is the thickness of the stator yoke,  $E$  is the elastic modulus,  $v$  is the spatial order of radial force harmonics,  $\sigma_v$  is the amplitude of  $v$ th-order radial force harmonics,  $\zeta_m$  is the modal damping,  $f_m$  is the modal angular frequency, and  $f_v$  is the angular frequency of radial force. As seen from eq. (8), when the radial force spatial order is larger than or equal to two, the vibration displacement is almost inversely proportional to the fourth power of the radial force spatial order. Therefore, the lowest-order radial force is considered to be the most significant vibration source.

The process of radial force harmonics acting on the stator teeth can be regarded as equidistant sampling. According to the Nyquist-Shannon sampling theorem, the modulated radial force can be expressed as

$$\begin{cases} p_m(\theta, t) = \sigma_r \cos(v\theta + 2\pi f_v t + \varphi_v), & v \leq \frac{Q}{2}, \\ p_m(\theta, t) = \sigma_r \cos(|v - kQ|\theta + 2\pi f_v t + \varphi_v), & v > \frac{Q}{2}, \end{cases} \quad (9)$$

where  $p_m$  is the modulated radial force density,  $\sigma_r$  and  $\varphi_r$  are the amplitude and phase of  $v$ th-order modulated radial force. When the radial force order  $v > Q/2$ , the  $v$ th-order radial force will be modulated to the  $(v - kQ)$ th-order one. Therefore, simply considering the radial force produced by the interaction between flux density harmonics is not sufficient. The force modulation effect can change the radial force spatial order, so as the vibration performance.

Figure 1 shows the radial force modulation process of the  $Q$ th-order radial force in integral-slot SPM machines. Since the spatial order of the  $Q$ th-order radial force is equal to the stator tooth number, the radial force acting on each stator tooth is the same. Therefore, the modulated  $Q$ th-order radial force presents a zeroth-order mode in the spatial distribution.

As mentioned above, the  $kQ$ th-order radial force can be modulated to the zeroth-order radial force. As seen in eq. (7), the  $kQ$ th-order radial force is produced by the  $v_p p$ th-order and  $(kQ \pm v_p p)$ th-order flux density harmonic. The frequencies of the  $v_p p$ th-order and  $(kQ - v_p p)$ th-order flux density harmonics are  $v_p f_e$  and  $(kQ/p \pm v_p) f_e$ , respectively. Therefore, the frequency of the  $kQ$ th-order radial force is  $k(Q/p) f_e$ . The radial force modulation only changes the spa-

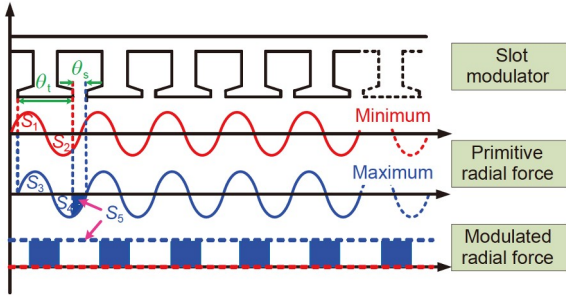


**Figure 1** (Color online) Force modulation process of  $Q$ th-order radial force in integral-slot SPM machines.

tial order of radial force, and it does not change the frequency. The frequency of the modulated zeroth-order radial force is consistent with that of the  $kQ$ th-order radial force before modulation.

As shown in **Figure 1**, the  $Q$ th-order primitive radial force harmonics are uniformly and continuously distributed in the air gap. However, when the force acts on the stator teeth surface, the radial force is discretized due to the slotted structure. The resultant force on a tooth is obtained by integrating the distributed force in a tooth pitch, and it can be written as

$$F_{r,q}(t) = \int_{(k-1)(\theta_t+\theta_s)+\frac{\theta_s}{2}}^{k(\theta_t+\theta_s)-\frac{\theta_s}{2}} LR_i p_r(\theta, t) d\theta$$

$$= \begin{cases} \int_{(k-1)(\theta_t+\theta_s)+\frac{\theta_s}{2}}^{k(\theta_t+\theta_s)-\frac{\theta_s}{2}} LR_i(p_m(\theta, t))d\theta, & v \leq \frac{Q}{2}, \\ \int_{(k-1)(\theta_t+\theta_s)+\frac{\theta_s}{2}}^{k(\theta_t+\theta_s)-\frac{\theta_s}{2}} LR_i(p_m(\theta, t))d\theta, & v > \frac{Q}{2}, \end{cases} \quad (10)$$

where  $F_{r,q}$  is the resultant force,  $L$  is the stack length of the stator,  $\theta_s$  is the slot opening pitch, and  $\theta_t$  is the stator tooth pitch. The slot opening width is related to the integral range of the radial force, so it affects the amplitude of the modulated radial force. The slot opening ratio is defined as

$$h = \frac{\theta_s}{\theta_t + \theta_s}. \quad (11)$$

As seen in **Figure 1**, when the positive half period and the negative half period of the radial force harmonic acting on the stator tooth are equal, the modulated radial force takes the minimum value, i.e., zero. When the stator tooth width is exactly half of a period of radial force, the amplitude of the modulated radial force harmonic is the largest. In such case, the relationship among the slot opening ratio, the slots number, and the radial force spatial order can be expressed as

$$\frac{v}{Q} \cdot (1-h)\Delta T v = \frac{1}{2}\Delta T v. \quad (12)$$

Therefore,

$$h = 1 - \frac{Q}{2v}. \quad (13)$$

The first waveform of primitive radial force in **Figure 1**

represents the moment when the resultant radial force on each stator tooth is zero, namely  $S_1=S_2$ . The second waveform of primitive radial force represents the moment when the resultant radial force has the greatest amplitude, and the resultant radial force on the stator tooth is equal to the area of  $S_3-S_4$ , i.e., the area of  $S_5$ . In such case, the amplitude of the modulated zeroth-order radial force can be expressed as

$$A_{r0} = S_5 = \int_0^{\theta_s} p_r d\theta. \quad (14)$$

The modulated zeroth-order radial force of the integral-slot SPM machine can be written as

$$p_{m0}(\theta, t) = A_{r0} \cos[0\theta - (2\pi Q/p)f_e t]$$

$$= \int_0^{\theta_s} (p_r \sin\theta) d\theta \cdot \cos[0\theta - (2\pi Q/p)f_e t]$$

$$= p_r (1 - \cos\theta_s) \cdot \cos[0\theta - (2\pi Q/p)f_e t], \quad (15)$$

where  $p_{m0}$  is the modulated zeroth-order radial force. **Figure 2** shows the relationship between the slot opening ratio and the modulated radial force amplitude of integral-slot SPM machines. With the increase of the slot opening ratio, the amplitude of the modulated radial force increases continuously until the slot opening ratio reaches 0.5. When the slot opening ratio is greater than 0.5, the amplitude of the modulated radial force on each stator tooth will decrease with the increase of the slot opening ratio.

### 3 Dummy slots design

In **Sect. 2**, the magnetic field modulation effect and radial force modulation caused by the slot slotting effect are studied, and the effect of slot opening width on the amplitude of modulated force is also investigated. In the next two sections, a 36-slot/12-pole integral-slot SPM machine will be taken as an example for illustration. Two new designs to reduce the  $Q$ th-order radial force will be proposed.

**Figure 3** shows the finite-element model of the 36-slot/12-pole integral-slot SPM machine with the dummy slots design. The width and height of the dummy slot are set to be 1 and 2 mm, respectively. The main parameters of the 36-slot/12-pole SPM machine are listed in **Table 1**. The  $B-H$  curve of the electrical steel is shown in **Figure 4**.

#### 3.1 Magnetic field and radial force

According to **eq. (9)**, the slot number is associated with the spatial order of the modulated magnetic field and modulated radial force. The dummy slots are designed to investigate the effect of slot numbers on the spatial order of the modulated magnetic field and radial force.

The dummy slots design was generally used to reduce the cogging torque and torque ripple of SPM machines [25], but it will sacrifice certain amount of average output torque.

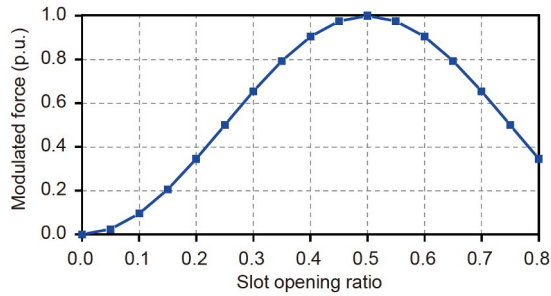


**Figure 2** (Color online) Modulated force varies with the slot opening ratio of integral-slot SPM machines.

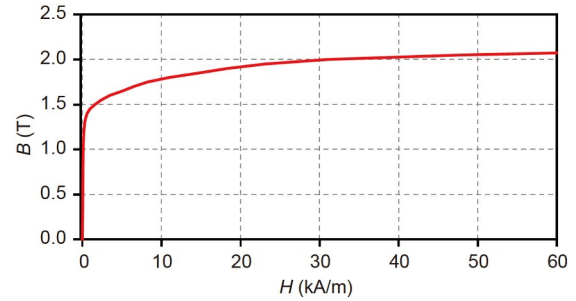


**Figure 4** (Color online)  $B$ - $H$  curve of the electrical steel.

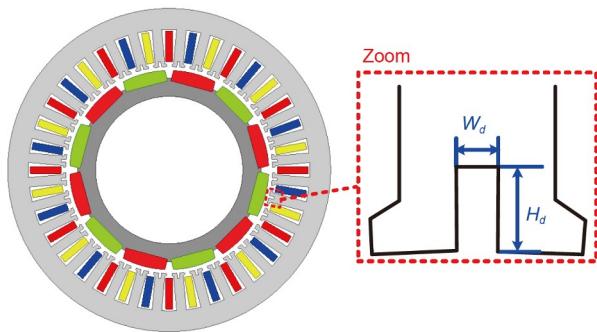


**Figure 3** (Color online) Finite-element model of 36-slot/12-pole integral-slot SPM with dummy slots design.

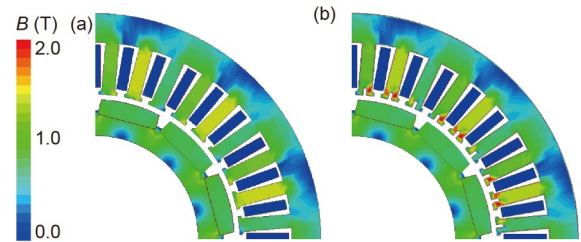


**Figure 5** (Color online) Flux density distribution. (a) Conventional; (b) dummy slot.

**Table 1** Main parameters of 36-slot/12-pole integral-slot SPM machine

Items	Symbol	Value
Stator outer diameter (mm)	$D_o$	125
Stator Inner diameter (mm)	$D_i$	80
Yoke thickness (mm)	$h_{yoke}$	8
Stack length (mm)	$L$	90
Air gap length (mm)	$g$	1.0
Slot opening (mm)	$s_o$	2
Thickness of PM (mm)	$h_{pm}$	5
PM remanence (T)	$B_{pm}$	1.09
Coercivity of PM (kA/m)	$H_c$	-800
Lamination material	-	DW310_35
Pole embrace	emb	0.83
Speed (r/min)	$n$	1000
Electrical frequency (Hz)	$f_e$	100

**Figure 5** shows the flux density distributions of conventional and dummy slots SPM machines under the rated load condition. Since the slotting effect reduces the area of the stator teeth, the flux density of the teeth tips of the slotted SPM machine is slightly larger than that of the conventional counterpart. **Figure 6** compares the torque of two SPM machines with conventional and dummy slots. The average output torque of the dummy slots SPM machine is only 0.2 N m lower than that of the conventional one, i.e., 1.5%.

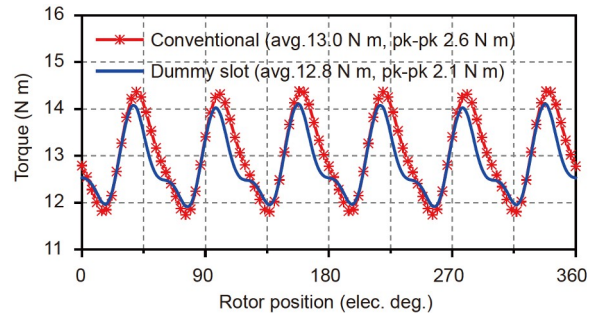


**Figure 6** (Color online) Torque comparison between two SPM machines.

The peak to peak torque of the dummy slots SPM machine has been decreased by 0.5 N m, i.e., 21.3%.

**Figure 7** shows the PM flux density of the 36-slot/12-pole SPM machines with different stator structures. The difference in flux density waveform of the 36-slot/12-pole SPM machines with conventional and dummy slots is noted in **Figure 7(a)**. As can be seen in **Figure 7(b)**, when the dummy slots design changes the air-gap permeance, the  $(Q \pm p)$ th-order flux density harmonics are effectively suppressed while the  $(2Q \pm p)$ th-order flux density harmonics are increased. **Figure 8** shows the radial force density spectrum of the two 36-slot/12-pole SPM machines under the open-circuit condition. The 36th-order radial force is reduced from 5.7 to 1.34 N/cm<sup>2</sup>, with a decrease of 76.5%. In addition, the amplitude of 72nd-order radial force increases by 34.7%, due to the increase of the  $(2Q \pm p)$ th-order flux density. It is worth noting that both 36th- and 72nd-order radial force harmonics

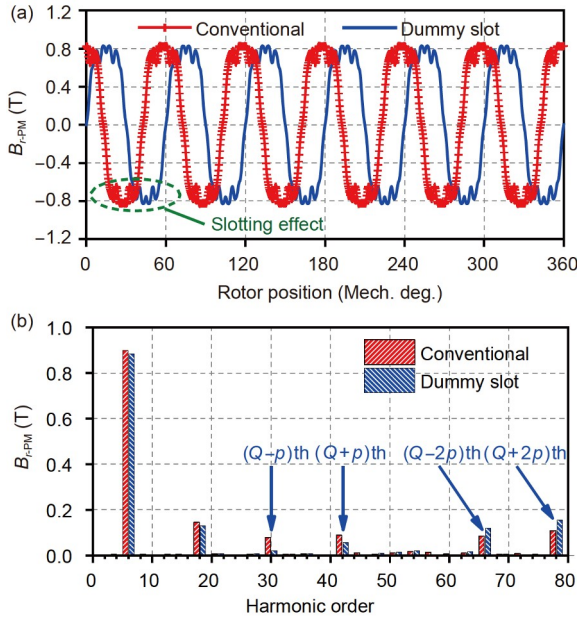


Figure 7 (Color online) Flux density of two machines. (a) Waveform; (b) spectrum.

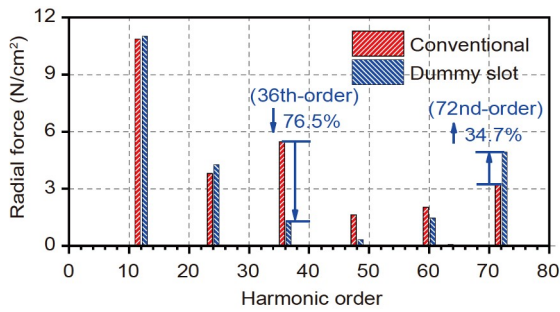


Figure 8 (Color online) Radial force spectrums of two machines.

can be modulated to the zeroth-order radial force harmonics, but their frequencies are different. The frequency of the 36th-order radial force is  $6f_e$ , while the frequency of the 72nd-order radial force is  $12f_e$ .

### 3.2 Verification of vibration reduction

The vibration of the SPM machine is the synthesis of all modes excited by all radial force harmonics. It can be calculated based on the modal superposition method, and it can be expressed as

$$[M] \sum_i^N \{\Phi_i\} \ddot{x}_i + [C] \sum_i^N \{\Phi_i\} \dot{x}_i + [K] \sum_i^N \{\Phi_i\} x_i = \{F_v(\theta, t)\}, \quad (16)$$

where  $[C]$  is the damping matrix,  $[K]$  is the stiffness matrix,  $[M]$  is the mass matrix,  $F_v$  is the exciting force,  $\{\Phi_i\}$  is the modal shape,  $x$  is the vibration displacement,  $i$  is a positive

integer, and  $N$  is the number of modes involved in the calculation. The synthetic vibration deformation and acceleration can be written as

$$x = \sum_{i=1}^N \{\Phi_i\} \cdot \eta_i, \quad (17)$$

$$\ddot{x} = -\omega_v \dot{x} = \omega_v^2 x. \quad (18)$$

The vibration prediction process of the SPM machine is a complex multi-physics issue. The multi-physics vibration prediction model is established as shown in Figure 9, which integrates three parts, i.e., the radial force calculation module, modal analysis module, and vibration calculation module. It should be emphasized that the actual modal damping and orthotropic material parameters can be obtained by a modal test, which will be carried out in Sect. 5.

Figure 10 shows the vibration acceleration spectrum of the 36-slots/12-pole SPM machines with different stator structures. It can be seen that the vibration peaks appear at  $6f_e$  and  $12f_e$ . It proves that the  $Q$ th-order and  $2Q$ th-order radial forces are the most critical components for the vibrations of the integral-slot SPM machine. As compared with that of the conventional SPM machine, the vibration acceleration of the dummy slots SPM machine has been significantly reduced at the frequency of  $6f_e$ . The decrease of vibration acceleration at the frequency of  $6f_e$  can be explained from two aspects. First, the decrease of the  $(Q \pm p)$ th-order flux density leads to the decrease of the  $Q$ th-order radial force. Second, the number of

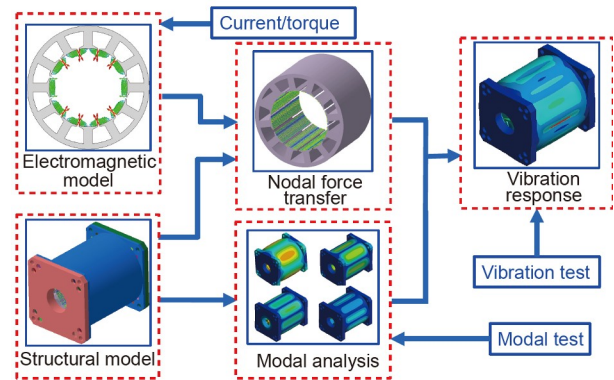


Figure 9 (Color online) Multiphysics vibration prediction model.

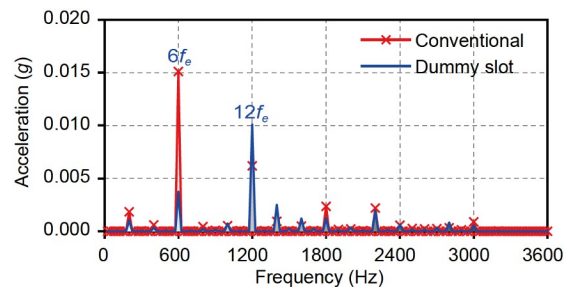


Figure 10 (Color online) Vibration simulation of two SPM machines.

slots is doubled due to the dummy slots design. The  $Q$ th-order radial force cannot be modulated to zeroth-order radial force by  $2Q$  stator teeth. However, due to the increase of the  $2Q$ th-order radial force, the vibration acceleration increases at the frequency of  $12f_e$ .

### 4 Bread-loaf magnets design

#### 4.1 Magnetic field and radial force

The dummy slots design reduces the 36th-order radial force of the 36-slot/12-pole SPM machine, but it increases the 72nd-order radial force. In order to get a better effect to reduce the radial force harmonics, it is necessary to analyze the critical flux density harmonic sources of the  $kQ$ th-order radial force. For example, to generate a 36th-order radial force, the spatial order of the two flux densities must be satisfied:

$$|v_1 \pm v_2| = 36, \quad v_1, v_2 \subseteq \{6, 18, 30, 42, \dots, (2k-1)p\}. \quad (19)$$

Tables 2 and 3 list the amplitudes and phases of the 36th- and 72nd-order radial force harmonics, which are produced by different flux density harmonics combinations. It can be seen that the relatively large radial force is mainly produced by the interaction between the flux density harmonics and the working harmonics (i.e., the 6th-order flux density). In addition, the flux density harmonics contribute to the 36th- and 72nd-order radial force in varying degrees.

Figure 11 shows the finite-element models of the 36-slot/12-pole SPM machines with conventional and bread-loaf magnets. All parameters of the two SPM machines are consistent except for the shape of the magnets. Figure 12 shows the torque performances of two 36-slot/12-pole SPM machines with different magnets. Compared with that of the conventional SPM machine, the average output torque of the

SPM machine with bread-loaf magnets decreases 0.9 N m, i.e., 6.9%. In addition, the peak to peak torque of the SPM machine with bread-loaf magnets has been decreased by 2.3 N m, i.e., 88.5%. Figure 13 shows the PM flux density of the 36-slots/12-pole SPM with different magnet structures. The SPM machine with bread-loaf magnets has a more si-

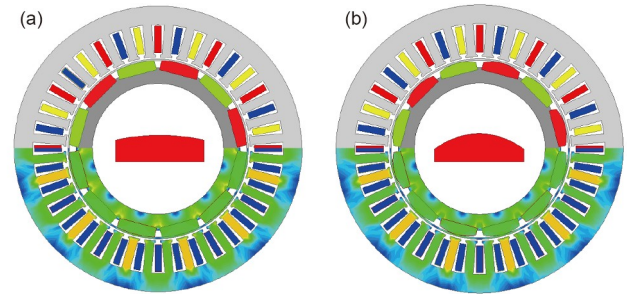


Figure 11 (Color online) SPM machines with different magnet structures. (a) Conventional one; (b) bread-loaf one.

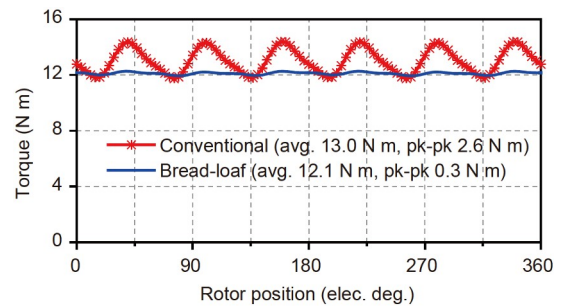


Figure 12 (Color online) Torque comparison between two machines with different magnets.

Table 2 Main source of 36th-order radial force

Source	Radial force (N/cm <sup>2</sup> )	Amplitude (N/cm <sup>2</sup> )	Phase (°)
( $v_1=6, v_2=30$ )	$-4.29+6.22e^{-4}i$	4.29	180
( $v_1=6, v_2=42$ )	$3.17+4.68e^{-4}i$	3.17	0
( $v_1=18, v_2=18$ )	$-2.82-1.15e^{-4}i$	2.82	180
( $v_1=18, v_2=54$ )	$0.76-8.6e^{-5}i$	0.76	0
( $v_1=30, v_2=66$ )	$0.22-6.3e^{-5}i$	0.22	0

Table 3 Main source of 72nd-order radial force

Source	Radial force (N/cm <sup>2</sup> )	Amplitude (N/cm <sup>2</sup> )	Phase (°)
( $v_1=6, v_2=66$ )	$3.69-1.29e^{-4}i$	3.69	0
( $v_1=6, v_2=78$ )	$4.08-2.17e^{-4}i$	4.08	0
( $v_1=18, v_2=54$ )	$0.76-0.86e^{-4}i$	0.76	0
( $v_1=18, v_2=90$ )	$0.46-0.09e^{-4}i$	0.46	0
( $v_1=30, v_2=42$ )	$0.19+0.07e^{-4}i$	0.19	0

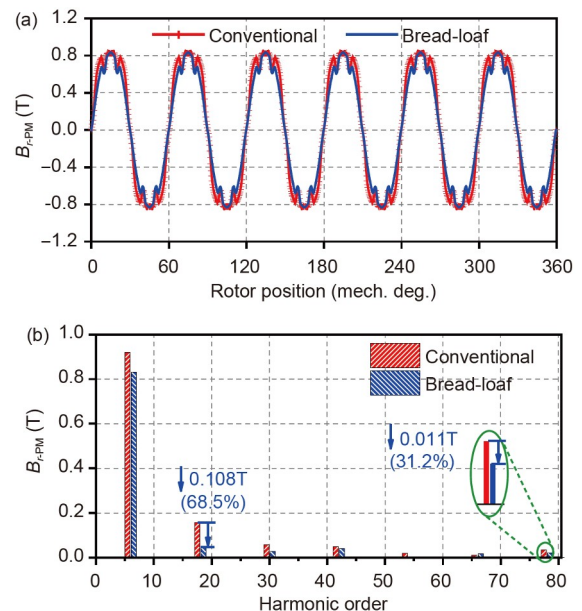


Figure 13 (Color online) PM flux densities. (a) Waveform; (b) spectrums.

nusoidal waveform than that with the conventional magnets structure. Figure 13(b) shows the spectrums of the flux density of the two SPM machines. The SPM machine with bread-loaf magnets significantly reduces the amplitude of each flux density harmonic. Especially, the 18th- and 78th-order flux density harmonics decreased by 68.5% and 31.2%, respectively, which undoubtedly benefit to reduce the 36th- and 72nd-order radial forces.

Figure 14 shows the 2D spectrums of radial force of two SPM machines with conventional and bread-loaf magnets. The red marks indicate the spatial order, frequency, and amplitude of the radial force harmonics. Compared with that of the 36-slot/12-pole SPM machine with conventional magnets, the amplitudes of 36th-order and 72nd-order radial force of the bread-loaf magnets SPM machine have been greatly reduced, by 88.5% and 78.3%, respectively. The reductions of the 36th-order and 72nd-order radial forces benefit from the suppression of flux density harmonics by the design of the bread-loaf magnet.

#### 4.2 Verification of vibration reduction

Figure 15 shows the vibration displacements caused by the 36th-order radial force of 36-slot/12-pole SPM machines with conventional and bread-loaf magnets. Although they are both excited by the 36th-order radial force, they show the zeroth-order vibration mode. It should be noted that due to the setting of constraints and the fact that the housing is not a cylindrical structure, the zeroth-order vibration mode cannot be observed. Its vibration shape is the so-called breath mode. In addition, the 36-slot/12-pole SPM machine with the bread-loaf magnets reduces the 36th-order radial force, which effectively weakens the vibration of the SPM machine.

Figure 16 shows the vibration acceleration spectrum of the 36-slots/12-pole SPM machines with different magnets. The vibration peaks appear at frequencies of  $6f_e$  and  $12f_e$ . It proves that the  $Q$ th-order and  $2Q$ th-order radial forces are the most critical components for the vibrations of the integral-slot SPM machine. In addition, compared with that of the SPM machine with conventional magnets, the vibrations of the bread-loaf SPM machine have been significantly reduced at frequencies of  $6f_e$  and  $12f_e$ , which benefits from the decrease of 36th-order and 72nd-order radial forces.

### 5 Experimental verifications

In order to verify the theoretical analysis and finite-element results, the 36-slot/12-pole integral-slot SPM machines are fabricated and tested. Although the dummy slots design reduces the  $Q$ th-order radial force of the SPM machine, the dummy slots design increases the  $2Q$ th-order radial force.

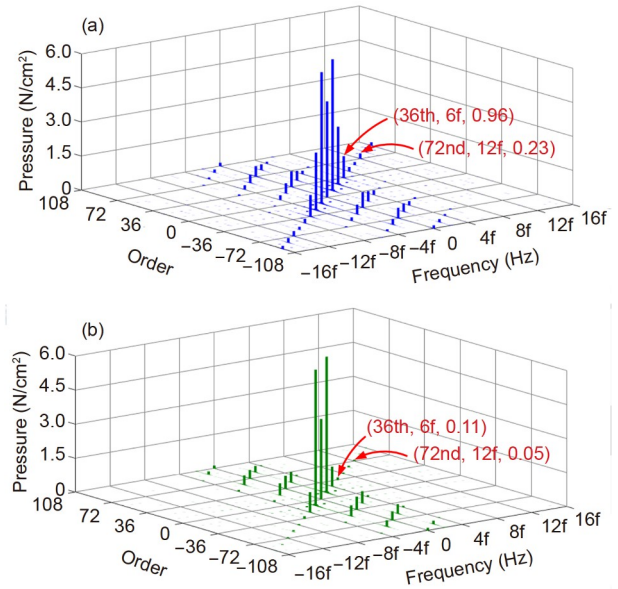


Figure 14 (Color online) 2D spectrums of radial force of two SPM machines with different magnet structures. (a) Conventional; (b) bread-loaf.

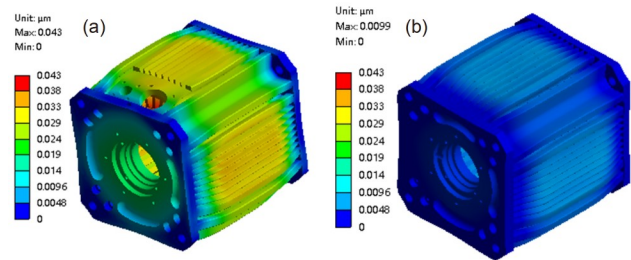


Figure 15 (Color online) Vibration caused by 36th-order radial force. (a) Conventional; (b) bread-loaf.

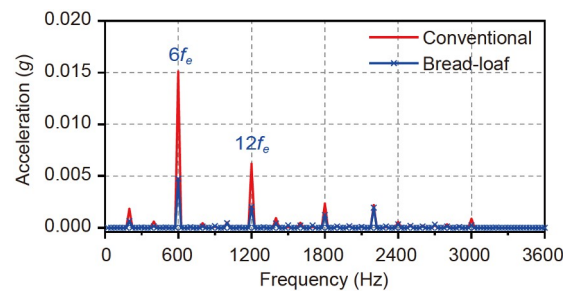


Figure 16 (Color online) Simulated vibration spectrums of two SPM machines with different magnets.

The vibration at the frequency of  $12f_e$  also increases. The bread-loaf magnets design has a good effect on weakening the  $Q$ th-order and  $2Q$ th-order radial forces, and the vibrations at frequencies of  $6f_e$  and  $12f_e$  are reduced. In addition, the bread-loaf magnets SPM machine has a lower torque ripple than the dummy slots SPM machine. Therefore, only the conventional and bread-loaf magnets SPM machines are fabricated and tested.



### 5.1 Prototype and modal test

Figure 17 shows the prototype of the 36-slot/12-pole integral-slot SPM machine. The modal test of the stator, stator with coils, stator assembly, and entire SPM machine are carried out to obtain the natural frequencies. The SPM machine is suspended by elastic ropes to simulate an unconstrained state as shown in Figure 18. The hammering method is used in this modal experiment. The integral electronic piezoelectric linear vibration accelerometer is used. The sensitivity, measured frequency, and measured range of the accelerometers are 500 mV/g, 0.2 Hz–10 kHz, and 0–100g, respectively, where  $g$  is the gravitational acceleration. Since the difference between two 36-slot/12-pole SPM machines is simply in magnet structure, the modal parameters of the two SPM machines are considered the same. Therefore, the modal experiment of only one 36-slot/12-pole SPM machine is conducted. By hammering multiple positions on the housing surface and picking up the corresponding vibration data, the frequency response function of the SPM machine is obtained.

Table 4 lists the modal parameters obtained by modal test and simulation. The errors of the 2nd-, 3rd- and 4th-order experimental and simulated modal frequencies are 3.02%, 2.19%, and 0.56%, respectively. It should be noted that the parameters of anisotropic materials in the modal simulation are obtained from modal experiments. The equivalent material parameters can be obtained by adjusting the parameters in the finite-element model to approximate the modal test results. The equivalent material parameters of the stator core, windings, and housing are given in Table 5.

### 5.2 Vibration response

In order to validate the theoretical vibration performance of 36-slot/12-pole integral-slot SPM machines, the vibration experiments of 36-slot/12-pole SPM machines with con-

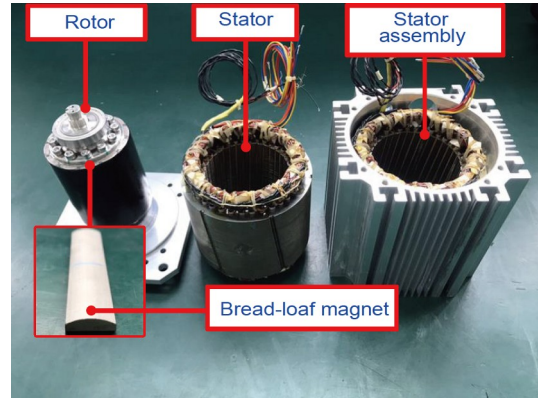


Figure 17 (Color online) Prototype of 36-slot/12-pole SPM machines.

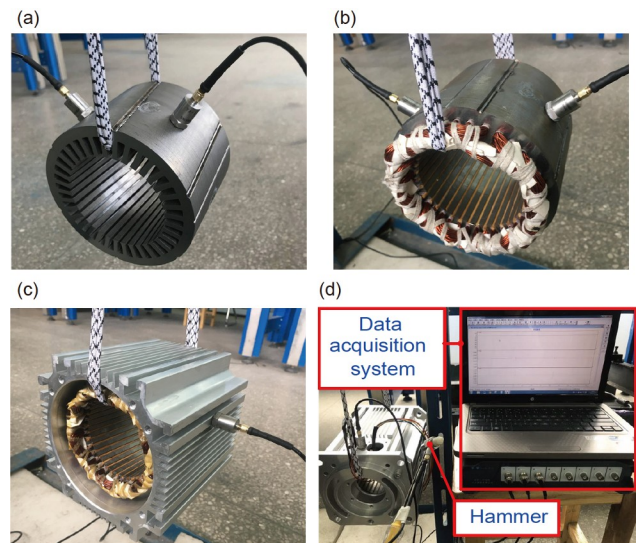
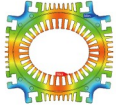




Figure 18 (Color online) Modal test of 36-slot/12-pole SPM machines. (a) Stator; (b) stator with coils; (c) stator assembly; (d) entire machine.

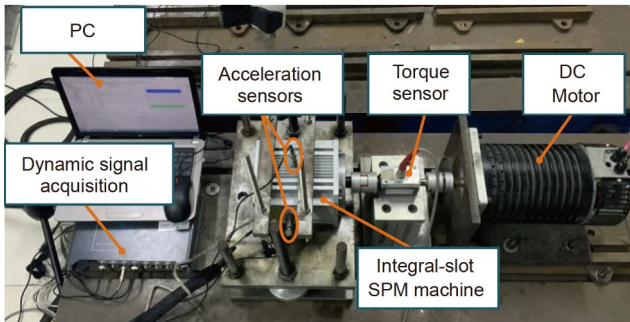
ventional and bread-loaf magnets are conducted. The vibration investigated in this paper is the linear vibration on the housing surface of the PM machines. Figure 19 shows the

Table 4 Modal parameters

Spatial order	Modal Shape	Simulated frequency (Hz)	Tested frequency (Hz)	Relative error (%)
2		2250	2318	3.02
3		4355	4450	2.19
4		6836	6874	0.56

**Table 5** Equivalent material properties

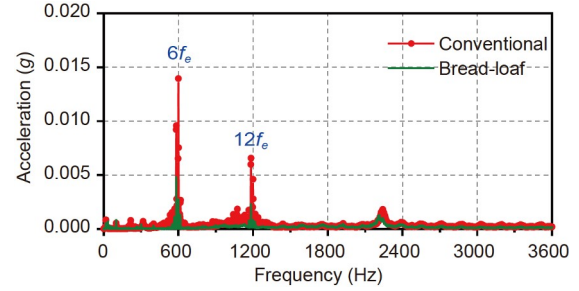
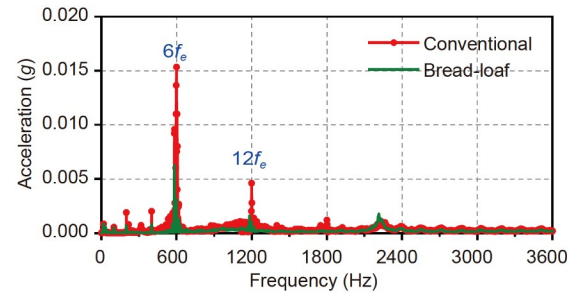
Items	Symbol	Stator core	Windings	Housing
Density ( $\text{kg/m}^3$ )	$\rho$	7860	5822	2770
Young's modulus (GPa)	$E_x$	205	0.2	
	$E_y$	205	0.2	70
	$E_z$	170	1	
Shear modulus (GPa)	$G_{xy}$	55	0.1	
	$G_{yz}$	26.5	0.14	25.6
	$G_{xz}$	26.5	0.14	
Poisson's ratio	$\nu_{xy}$	0.3	0.2	
	$\nu_{yz}$	0.27	0.1	0.33
	$\nu_{xz}$	0.27	0.1	

**Figure 19** (Color online) Experimental device of vibration test.

vibration experimental devices of the 36-slot/12-pole SPM machines.

Figure 20 shows the experimental results of vibration acceleration of the 36-slot/12-pole SPM machines with conventional and bread-loaf magnets under the open-circuit condition. The SPM machines rotate at 1000 r/min in the test. Hence, the fundamental electric frequency is 100 Hz. There are three vibration peaks in Figure 20, i.e., at 600, 1200, and 2250 Hz. For the integral-slot SPM machines, the most significant factor for the vibration is the zeroth-order radial force modulated from  $kQ$ th-order radial forces, and the frequencies are  $k(Q/p)f_e$ . For the 36-slot/12-pole SPM machine, 600 and 1200 Hz are the  $6f_e$  and  $12f_e$ , respectively. Compared with that of the conventional SPM machine, the vibration acceleration of the SPM machine with the bread-loaf magnets decreases by 65.7% and 64.9% at 600 and 1200 Hz, respectively. In addition, since the  $kQ$ th-order radial force amplitude with  $18f_e$  and later frequencies are very small, they have little effect on generating vibrations.

Figure 21 shows the experimental results of vibration acceleration of the two SPM machines under the rated load condition. Since the integral-slot SPM machine has a low content of armature reaction flux density harmonics, the vibration at the frequency of  $6f_e$  increases slightly under the rated load condition. As shown in Tables 2 and 3, the total

**Figure 20** (Color online) Experimental vibration under open-circuit conditions.**Figure 21** (Color online) Experimental vibration under rated load conditions.

radial force is composed of numerous harmonics with different phases. The phase of the radial force harmonics generated by the armature reaction flux density can be opposite to that generated by the PM flux density, which will cause the total radial force amplitude under the loaded condition to be lower than that under the open-circuit condition. It can be seen that the vibration at the frequency of  $12f_e$  under the rated load condition is lower than that under the open-circuit condition. In addition, both simulated and experimental results in Table 4 show that there is a resonance frequency of the SPM machine at around 2300 Hz. Therefore, it can be judged that the vibration peak around 2300 Hz is caused by the 2nd-order mode. The 36-slot/12-pole SPM machine with bread-loaf magnets effectively reduces the vibrations. The experimental results are well agreed with the above theoretical analyses.

## 6 Conclusions

In this paper, two different designs for SPM machines, with dummy slots and bread-loaf magnets techniques, are presented. The proposed designs can reduce the electromagnetic vibration in integral-slot SPM machines, with consideration of the radial force modulation. Firstly, the stator slotting effect on the magnetic field and radial force modulation have been investigated. It reveals that the amplitude of the modulated radial force is affected by the slot opening width,

while the spatial order is associated with the slot numbers. Then, the influence of slot opening width on the radial force has been investigated, and it tends to take a small value to reduce the amplitude of the modulated radial force in the appropriate range. Afterwards, the dummy slots and bread-loaf magnets designs have been proposed to reduce the vibrations of a 36-slot/12-pole integral-slot SPM machine, and the vibration reduction principles have been elaborated in detail. The dummy slots design has a great effect on reducing the  $Q$ th-order radial force, but it has increased the  $2Q$ th-order radial force. However, the SPM machine with the bread-loaf magnets has reduced both the  $Q$ th-order and  $2Q$ th-order radial force.

Finally, two 36-slot/12-pole integral-slot SPM machines with conventional and bread-loaf magnets have been manufactured and tested to validate the theoretical analyses.

*This work was supported by the National Natural Science Foundation of China (Grant Nos. 51991383 and 52025073).*

- 1 Ma Y, Wang J, Zhou L, et al. Surrogate-assisted optimization of a five-phase SPM machine with quasi-trapezoidal PMs. *IEEE Trans Ind Electron*, 2022, 69: 202–212
- 2 Liu T, Zhao W, Ji J, et al. Effects of eccentric magnet on high-frequency vibroacoustic performance in integral-slot SPM machines. *IEEE Trans Energy Convers*, 2021, 36: 2393–2403
- 3 Zhu J, Zuo Y, Chen H, et al. Deep-investigated analytical modeling of a surface permanent magnet vernier motor. *IEEE Trans Ind Electron*, 2021, doi: 10.1109/TIE.2021.3134075
- 4 Dong Q C, Liu X T, Qi H Z, et al. Analysis and evaluation of electromagnetic vibration and noise in permanent magnet synchronous motor with rotor step skewing. *Sci China Tech Sci*, 2019, 62: 839–848
- 5 Ji Z, Cheng S, Lv Y, et al. The mechanism for suppressing high-frequency vibration of multiphase surface permanent magnet motors via PWM carrier phase shifting. *IEEE Trans Power Electron*, 2021, 36: 10504–10513
- 6 Zhu S, Zhao W, Liu G, et al. Effect of phase shift angle on radial force and vibration behavior in dual three-phase PMSM. *IEEE Trans Ind Electron*, 2021, 68: 2988–2998
- 7 Zou J, Lan H, Xu Y, et al. Analysis of global and local force harmonics and their effects on vibration in permanent magnet synchronous machines. *IEEE Trans Energy Convers*, 2017, 32: 1523–1532
- 8 Ito F, Takeuchi K, Kotsugai T, et al. A study on asymmetry of electromagnetic force modes of permanent magnet synchronous motors with rotor eccentricity. *IEEE Trans Magn*, 2021, 57: 1–6
- 9 Lu Y, Li J, Qu R, et al. Electromagnetic force and vibration study on axial flux permanent magnet synchronous machines with dual three-phase windings. *IEEE Trans Ind Electron*, 2020, 67: 115–125
- 10 Deng W, Zuo S. Electromagnetic vibration and noise of the permanent-magnet synchronous motors for electric vehicles: An overview. *IEEE Trans Transp Electrific*, 2019, 5: 59–70
- 11 Yang H, Chen Y. Influence of radial force harmonics with low mode number on electromagnetic vibration of PMSM. *IEEE Trans Energy Convers*, 2014, 29: 38–45
- 12 EL-Refaie A M. Fractional-slot concentrated-windings synchronous permanent magnet machines: Opportunities and challenges. *IEEE Trans Ind Electron*, 2010, 57: 107–121
- 13 Valavi M, Le Besnerais J, Nysveen A. An investigation of zeroth-order radial magnetic forces in low-speed surface-mounted permanent magnet machines. *IEEE Trans Magn*, 2016, 52: 1–6
- 14 Wang S, Hong J, Sun Y, et al. Analysis of zeroth-mode slot frequency vibration of integer slot permanent-magnet synchronous motors. *IEEE Trans Ind Electron*, 2020, 67: 2954–2964
- 15 Besnerais J. Vibroacoustic analysis of radial and tangential air-gap magnetic forces in permanent magnet synchronous machines. *IEEE Trans Magn*, 2015, 51: 8105609
- 16 Fang H, Li D, Guo J, et al. Hybrid model for electromagnetic vibration synthesis of electrical machines considering tooth modulation and tangential effects. *IEEE Trans Ind Electron*, 2021, 68: 7284–7293
- 17 Zhu S, Zhao W, Ji J, et al. Investigation of bread-loaf magnet on vibration performance in FSCW PMSM considering force modulation effect. *IEEE Trans Transp Electrific*, 2021, 7: 1379–1389
- 18 Wang S, Hong J, Sun Y, et al. Mechanical and magnetic pivot roles of tooth in vibration of electrical machines. *IEEE Trans Energy Convers*, 2021, 36: 139–148
- 19 Lin F, Zuo S G, Deng W Z, et al. Reduction of vibration and acoustic noise in permanent magnet synchronous motor by optimizing magnetic forces. *J Sound Vib*, 2018, 429: 193–205
- 20 Zhao W, Zhu S, Ji J, et al. Analysis and reduction of electromagnetic vibration in fractional-slot concentrated-windings PM machines. *IEEE Trans Ind Electron*, 2022, 69: 3357–3367
- 21 Ma J, Zhu Z Q. Mitigation of unbalanced magnetic force in a PM machine with asymmetric winding by inserting auxiliary slots. *IEEE Trans Ind Appl*, 2018, 54: 4133–4146
- 22 Jafarboland M, Farahabadi H B. Optimum design of the stator parameters for noise and vibration reduction in BLDC motor. *IET Electric Power Appl*, 2018, 12: 1297–1305
- 23 Wang S, Hong J, Sun Y, et al. Analysis and reduction of electromagnetic vibration of PM brush DC motors. *IEEE Trans Ind Applicat*, 2019, 55: 4605–4612
- 24 Zuo S, Lin F, Wu X. Noise analysis, calculation, and reduction of external rotor permanent-magnet synchronous motor. *IEEE Trans Ind Electron*, 2015, 62: 6204–6212
- 25 Zhao G, Hua W, Zhu X, et al. The Influence of dummy slots on stator surface-mounted permanent magnet machines. *IEEE Trans Magn*, 2017, 53: 1–5